Available online at www.scholarsresearchlibrary.com

Scholars Research Library

Der Pharmacia Lettre, 2015, 7 (1):54-66
(http://scholarsresearchlibrary.com/archive.html)

ISSN 0975-5071
USA CODEN: DPLEB4

A density functional study of the inhibition of microsomal prostaglandin E_2 Synthase-1 by 2-aryl substituted quinazolin-4(3*H*)-one, pyrido[4,3-*d*] pyrimidin-4(3*H*)-one and pyrido[2,3-*d*]pyrimidin-4(3*H*)-one derivatives

Matías S. Leal, Andrés Robles-Navarro and Juan S. Gómez-Jeria*

Quantum Pharmacology Unit, Department of Chemistry, Faculty of Sciences, University of Chile, Las Palmeras 3425, Santiago, Chile

---

ABSTRACT

Here we report the results of the application of a quantum-chemical model-based method to the uncovering of the electronic factors controlling the variation of the inhibitory activity of microsomal prostaglandin E_2 synthase-1 by 2-aryl substituted quinazolin-4(3H)-one, pyrido[4,3-d]pyrimidin-4(3H)-one and pyrido[2,3-d]pyrimidin-4(3H)-one derivatives. The electronic structure was calculated at the B3LYP/6-31G(d,p) level. Complementary docking studies were carried out with a crystal structure of human mPGES-1. We found a good relationship between the electronic structures and inhibitory activities and a partial pharmacophore was proposed. Our results suggest specific interactions between some atoms and unknown residues of the enzyme. Docking studies show what residues are available for these specific interactions.

Keywords: Microsomal prostaglandin E_2 synthase-1, atomic reactivity indices, QSAR, mPGES-1, DFT.

INTRODUCTION

Microsomal prostaglandin E_2 synthase-1 (mPGES-1) belongs to the superfamily of membrane-associated proteins implicated in eicosanoid and glutathione metabolism. It catalyzes the formation of prostaglandin E_2 (PGE_2) from the endoperoxide prostaglandin H_2 (PGH_2). The expression of this enzyme is provoked during the inflammatory response. In fact, mPGES-1 expression is upregulated in animal models of rheumatoid arthritis and in patients suffering from osteoarthritis and it is downregulated by anti-inflammatory compounds. Also, mPGES-1 has a role in several other disease conditions including bone disorders, cancer, fever, inflammation, pain and stroke [1-18]. It is known that some of the non-steroidal anti-inflammatory drugs target the prostaglandin pathway and inhibit cyclooxygenase COX-2. Unhappily, the inhibition of COX-2 blocks the functions of all downstream protaglandin synthases, including the conversion of PGH_2 to prostacyclin I_2 (PGI_2). The blockage of the production of PGI_2 seems to play a role in the cardiovascular side effects of some compounds. For this reason, the inhibition of mPGES-1 has emerged as a novel strategy which will target only the PGE_2 pathway [2, 19-21]. Inhibitors of mPGES-1 would then serve as valuable anti-inflammatory therapeutics, especially if they lack the side effects associated with the COX-2 inhibition. Several molecules have been synthesized and tested for mPGES-1 inhibition [22-53]. The knowledge of the microscopic factors controlling the binding of new ligands to mPGES-1 should provide information that could be helpful in the design of new compounds with enhanced inhibitory activity. Recently, a group of 2-aryl-substituted quinazolin-4(3*H*)-one, pyrido[4,3-*d*]pyrimidin-4(3*H*)-one and pyrido[2,3-*d*]pyrimidin-

4(3*H*)-one derivatives have been synthesized and tested for inhibition of the recombinant human mPGES-1 enzyme [27]. In this paper we report the results of the application of a quantum-chemical model-based method [54] to the detection of the electronic structural factors controlling the variation of the inhibitory activity in the abovementioned molecules. This study is complemented with an analysis of the docking of two of these molecules to microsomal prostaglandin E_2 synthase-1.

MATERIALS AND METHODS

The model employed here has been the theme of discussion in many papers and we only present here a résumé of the final result of its development. Any drug-site equilibrium constant, expressed indirectly as IC_{50}, can be written in terms of the following set of reactivity indices [55-61]:

$$\log(IC_{50}) = a + \sum_j \left[e_j Q_j + f_j S_j^E + s_j S_j^N \right] +$$
$$+ \sum_j \sum_m \left[h_j(m) F_j(m) + x_j(m) S_j^E(m) \right] + \sum_j \sum_{m'} \left[r_j(m') F_j(m') + t_j(m') S_j^N(m') \right] +$$
$$+ \sum_j \left[g_j \mu_j + k_j \eta_j + o_j \omega_j + z_j \varsigma_j + w_j Q_j^{\max} \right] + \sum_{B=1}^{W} O_B \qquad (1)$$

where a, e_j, f_j, s_j, etc., are constants to be determined. Q_j, S_j^E and S_j^N are, respectively, the net charge, the total atomic electrophilic superdelocalizability and the total atomic nucleophilic superdelocalizability of atom j. $F_j(m)$ and $F_j(m')$ are, respectively, the Fukui indexes of occupied molecular orbital (MO) m and vacant MO m' localized on atom j. $S_j^N(m')$ is the local (orbital) atomic nucleophilic superdelocalizability of vacant MO m' localized on atom j. $S_j^E(m)$ is the local (orbital) atomic electrophilic superdelocalizability of occupied MO m localized on atom j. μ_j, η_j, ω_j and ς_j are, respectively, the local atomic electronic chemical potential, the local atomic hardness, the local atomic softness and the local atomic electrophilicity of atom j. $Q_j^{\max}$ is the maximal amount of charge atom j may receive [60, 61]. O_B is the orientational parameter of substituent B, an entirely geometrical term derived from the rotational partition function [58, 59]. As the physical meaning of the LARIs has been discussed in a number of papers, we refer the reader to the literature [62-82].

The set analyzed here is a group of 2-aryl substituted quinazolin-4(3*H*)-one, pyrido[4,3-*d*]pyrimidin-4(3*H*)-one and pyrido[2,3-*d*]pyrimidin-4(3*H*)-one derivatives with inhibitory activities against the recombinant human mPGES-1 enzyme [27]. The selected molecules and inhibitory activities (expressed as IC_{50}) are shown in Figure 1 and Table 1.

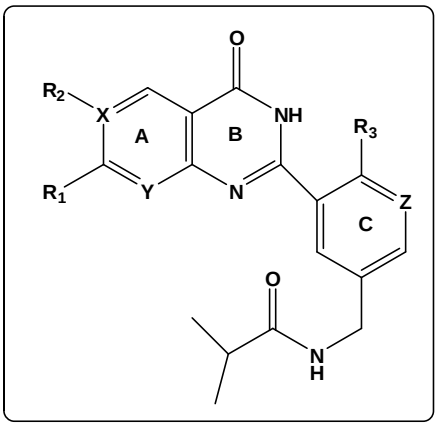

Figure 1. General formula of the molecules studied in this paper

Table 1. Structures and inhibitory activity

Mol.	R_1	R_2	R_3	X	Y	Z	log(IC_{50})
1	–Cl	–H	–Cl	C	C	C	1.62
2	–Br	–H	–Cl	C	C	C	1.56
3	$-CF_3$	–H	–Cl	C	C	C	1.41
4	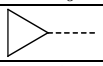	–H	–Cl	C	C	C	1.76
5	$-NO_2$	–H	–Cl	C	C	C	1.80
6	–OMe	–H	–Cl	C	C	C	2.48
7	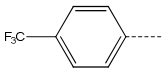	–H	–Cl	C	C	C	0.85
8	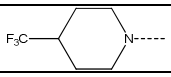	–H	–Cl	C	C	C	1.87
9	–H	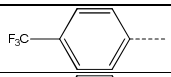	–Cl	C	C	C	1.74
10	–Cl	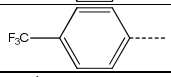	–Cl	C	C	C	1.56
11	–Cl	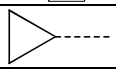	–Cl	C	C	C	1.51
12	–Cl	–OMe	–Cl	C	C	C	2.05
13	–Cl	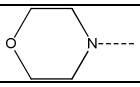	–Cl	C	C	C	2.42
14	–Cl	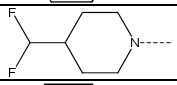	–Cl	C	C	C	1.38
15	–Cl		–Cl	C	C	C	2.68
16	–Cl	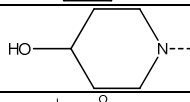	–Cl	C	C	C	2.85
17	–Cl	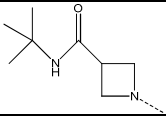	–Cl	C	C	C	1.77
18	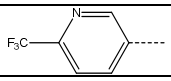	–H	–Cl	C	C	C	1.20

19	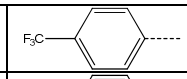	─H	─CHF_2	C	C	N	0.78
20	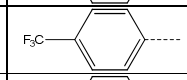	---	─Cl	N	C	C	0.70
21		─H	─Cl	C	N	C	1.00
22	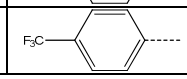	---	─CHF_2	N	C	N	0.60

Calculations

The electronic structure of all the molecules was calculated with Density Functional Theory at the B3LYP/6-311g(d,p) level using the Gaussian program [83]. After single point calculations, all the numerical values of the local atomic reactivity indices of Eq. 1 were calculated with the D-CENT-QSAR software [84]. Negative electron populations and MO populations greater than 2 produced by Mulliken Population Analysis were corrected as usual [85]. Orientational parameters were calculated as proposed [59]. Linear Multiple Regression Analysis (LMRA) techniques were used to find the best solution of Eq. 1. For each case, a matrix was built containing the logarithm of the dependent variable (IC_{50}) and the local atomic reactivity indices of all atoms of a common skeleton (a group of atoms, common to all molecules analyzed, and accounting for virtually all the biological activity; see Fig. 2 and [60, 86]) as independent variables. The Statistica software was used for LMRA [87]. Molecular orbitals and Molecular Electrostatic Potentials (MEP) were depicted using GaussView and Molekel software [83, 88].

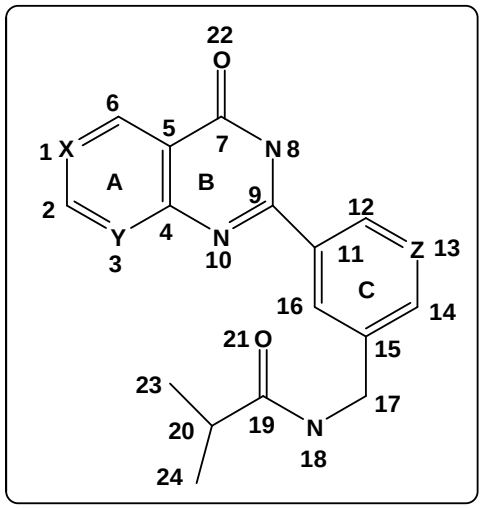

Figure 2. Common skeleton numbering

We employed Autodock 4 software for docking studies [89, 90]. A crystal structure of human mPGES-1 was downloaded from the Protein Data Bank (3DWW). Molecules 39 (the least active) and 50 (the most active) were selected for docking. The enzyme residues were kept rigid. A grid box with 50x54x62 points and a grid spacing of 0.375Å were used. For all procedures, 50 independent runs were carried out with a preliminary population of 300 randomly placed individuals, 50,000,000 energy evaluations and a maximum number of generations of 270,000. The results were clustered based on a 2.0 Å rmsd criterion. The selected structure for analysis was the one having the lowest energy in the largest cluster. Chimera was used for distance analysis and image processing.

RESULTS

An LRMA analysis including all molecules (n=22) did not produce a statistically significant equation and molecule 14 was detected as an outlier. When this molecule excluded from the set the following equation was obtained:

$$\log(IC_{50}) = 2.49 + 0.50S_1^E(HOMO-1)* - 2.23F_2(HOMO-1)* + 0.18S_{13}^E + 9.39F_9(LUMO+1)* - 6.29S_9^E(HOMO-1)* \quad (2)$$

with n=21, F(5,15)=112.11 (p<0.000001), R^2=0.97, adj. R^2=0.97, outliers>2σ=0 and SD=0.12. No outliers were detected and no residuals fall outside the ±2σ limits. Here, S_{13}^E is the total atomic electrophilic superdelocalizability of atom 13, $F_2(HOMO-1)*$ is the Fukui index [91] of the second highest occupied MO localized on atom 2, $F_9(LUMO+1)*$ is the Fukui index of the second lowest vacant MO localized on atom 9, $S_1^E(HOMO-1)*$ is the electrophilic superdelocalizability of the second highest occupied MO localized on atom 1 and $S_9^E(HOMO-1)*$ is the electrophilic superdelocalizability of the second highest occupied MO localized on atom 9. Tables 2 and 3 show, respectively, the beta coefficients, the results of the t-test for significance of coefficients and the matrix of squared correlation coefficients for the variables of Eq. 2. Table 3 shows that there are no important internal correlations between independent variables. Figure 3 displays the plot of observed *vs.* calculated log(IC_{50}) values. The associated statistical parameters of Eq. 2 show that this equation is statistically significant and that the variation of the numerical value of a group of five LARIs of atoms composing the common skeleton explains about 97% of the variation of the inhibitory capacity in this group of molecules.

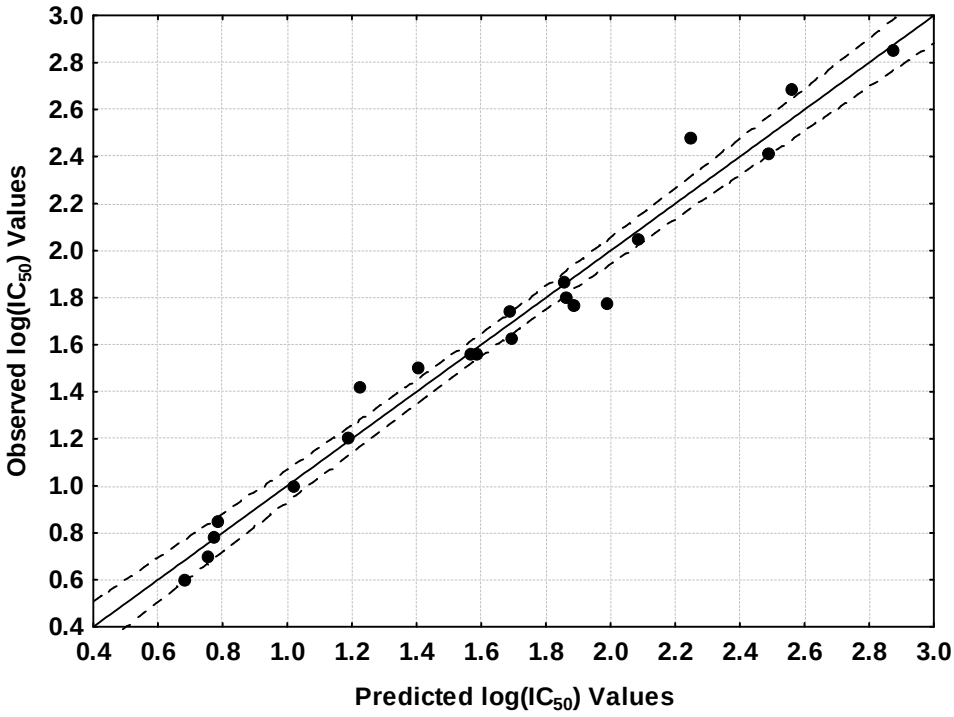

Figure 3. Plot of predicted *vs.* observed log(IC_{50}) values from Eq. 1. Dashed lines denote the 95% confidence interval

Table 2. Beta values and results of the t-test for significance of coefficients for the variables appearing in Eq. 2

	Beta	t(15)	p-level
$S_1^E(HOMO-1)*$	0.27	6.05	<0.00002
$F_2(HOMO-1)*$	-0.48	-9.32	<0.000001
S_{13}^E	0.23	5.11	<0.0001
$F_9(LUMO+1)*$	0.88	18.54	<0.000001
$S_9^E(HOMO-1)*$	-0.44	-10.24	<0.000001

Table 3. Matrix of squared correlation coefficients for the variables appearing in Eq. 2

	$S_1^E(HOMO-1)*$	$F_2(HOMO-1)*$	S_{13}^E	$F_9(LUMO+1)*$
$F_2(HOMO-1)*$	0.08	1.00		
S_{13}^E	0.004	0.16	1.00	
$F_9(LUMO+1)*$	0.004	0.16	0.04	1.00
$S_9^E(HOMO-1)*$	0.0004	0.0004	0.0008	0.03

Figures 4 and 5 show, respectively, molecules 39 (the least active) and 50 (the most active) docked to human mPGES-1. Table 4 displays some ligand-residue distances.

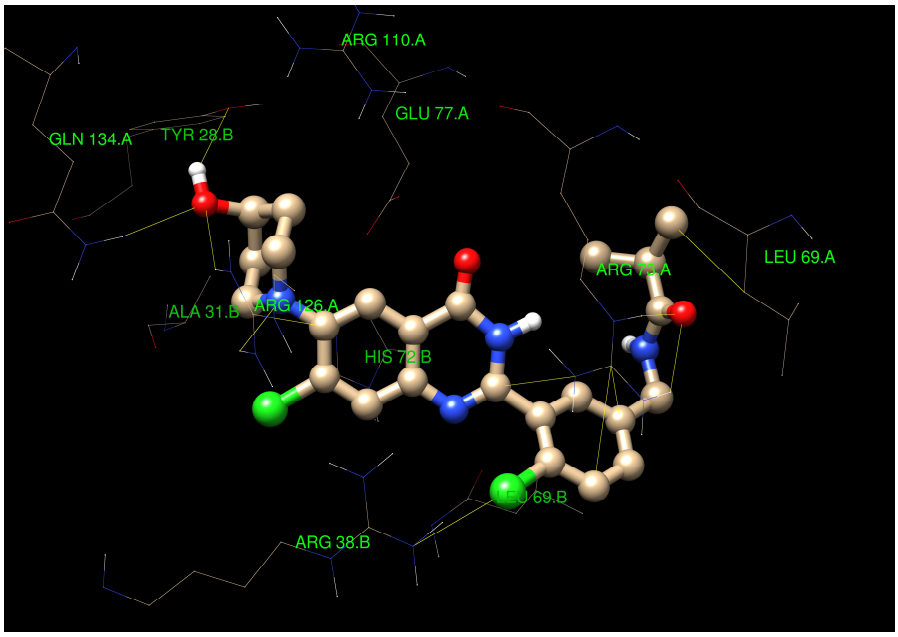

Figure 4. 39 docked to human mPGES-1

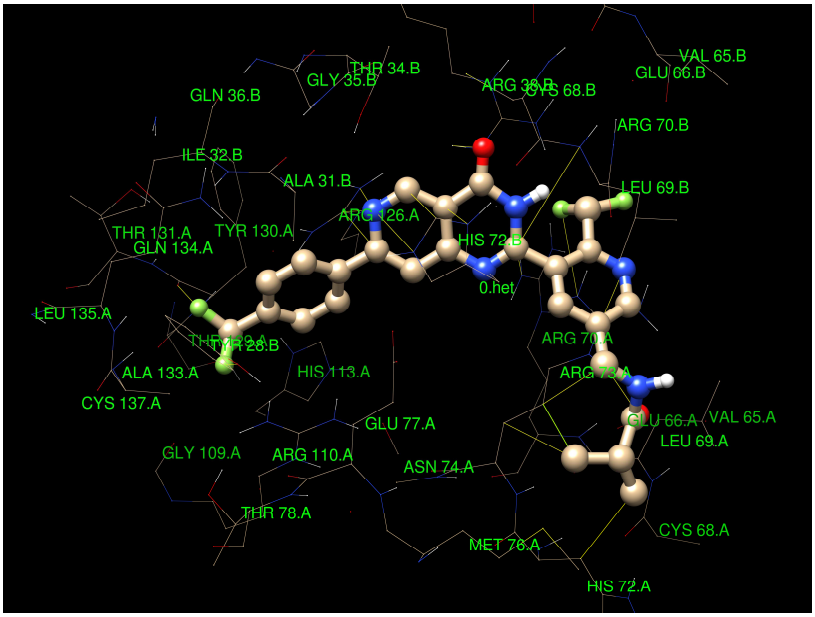

Figure 5. 50 docked to human mPGES-1

Table 4. Main ligand-residue distances.

Mol.	Main interactions (marked in yellow in Figs. 4-5)
39	C9-N from Arg-73A (3.56Å), O (from side chain)-HN from Arg-73A (1.84Å), O (from side chain)-NH from Arg-73A (2.73Å), O (from C1 subst.)-NH from Gln-134A (2.99Å), O (from C1 subst.)-NH from Arg-126A (3.66Å), OH (from C1 subst)-OH from Tyr-28B (2.18Å), N (from C1 subst.)-HN from Arg-126A (2.41Å), C1-C from Arg-126A (3.93Å), C2-C from His-72B (3.23Å), C12-C from Arg-73A (3.73Å), C13-C from Arg-73A (3.47Å), C24-C from Leu-69A (4.36Å) Cl-N from Arg-39B (3.39Å)
50	O22-H from Arg-38B (2.99Å), C9-N from Arg-70A (5.44Å) C9-N from Leu-69B (5.56Å), O (from side chain)-H from Arg-73A (1.95Å), F (from CHF_2)-N from Arg-73A (3.38Å), F (from CF_3)-O from Tyr-130A (2.68Å), C24-C from His-72A(3.33Å), C24-C from Arg-73A (3.27Å), C6-C from His-72B (3.38Å), N1-N from His-72B (3.78Å), C5-C from His-72B (4.01Å), C23-C from Arg-73A (3.89Å), N1-N from Arg-126A (2.7Å), C2-C from Arg-126A (3.67Å), F (from CF_3)-C from Arg-126A (3.59Å), F (from CF_3)-HN from Tyr-28B (2.32Å), C (from side chain)-N from Arg-73A (3.95Å), N13-C from Arg-73A (3.09Å)

DISCUSSION

The beta values (Table 2) indicate that the relative importance of these indices is $F_9(LUMO+1)^*$ >> $F_2(HOMO-1)^*$ > $S_9^E(HOMO-1)^*$ >> $S_1^E(HOMO-1)^*$ > S_{13}^E. A high mPGES-1 inhibitory capacity is then associated with high numerical values for $\left|S_1^E(HOMO-1)^*\right|$, $\left|S_{13}^E\right|$ and $F_2(HOMO-1)^*$ and with a small value for $F_9(LUMO+1)^*$ and $\left|S_9^E(HOMO-1)^*\right|$. Table 4 displays the local molecular orbital structure of atoms 1, 2 and 9 of the common skeleton.

Table 4. Local molecular orbital structure of atoms 1, 2 and 9 of the common skeleton

Mol.	Mol.	Atom 1	Atom 2	Atom 9
1	19	98π100π101π-102π105π107π	93π98π101π-102π103π105π	95σ97σ101π-102π105σ106σ
2	20	102σ103σ110π-111π112π114π	102σ108π110π-111π112π114π	104σ106σ110π-111π114σ116σ
3	21	101π104π109π-110π111π113π	101π104π109π-110π111π113π	103σ106σ109π-110π113σ114σ
4	22	97π103σ104π-105π108π111σ	96σ103π104π-106π108π111σ	98σ100σ104π-105π108σ109σ
5	23	97π98σ105π-106π109π110π	98σ104σ105π-106π107π109σ	101σ104σ105π-106π109σ110π
6	24	93π94π101π-102π104σ105π	92π100π101π-103π104π105σ	97σ100π101π-102π105σ106σ
7	28	121π128σ129π-130π133π134π	121π128π129π-130π131π134π	122σ125σ129π-130π131σ134π
8	29	126σ131π132π-133π135σ136π	124σ125π132π-134π135π136π	127σ129σ131π-133π136σ137σ
9	30	118σ119π129π-130π131σ132σ	124π125π129π-130π131π132π	123σ126σ129π-130π135σ136σ
10	31	127σ132σ137π-138σ139σ140σ	127σ134π137π-138π139π140σ	131σ132σ137π-138π143σ144σ
11	32	103σ105π112π-113π114σ116π	105π110π112π-113π 114π116σ	106σ108σ112π-113π116σ117σ
12	33	102π103σ109π-110π111σ113π	102π107π109π-111π113σ116σ	103σ105σ109π-110π113σ114σ
13	34	122π123σ124π-125π126σ128σ	114σ120π124π-126π128σ130σ	119σ123π124π-125π128σ129σ
14	35	134σ135σ136π-137π138π140σ	134π135σ136π-138π140π143σ	134π135π136π-137π140σ141σ
15	37	116π119σ121π-122π123σ125σ	116π117π121π-122π123σ125σ	112σ115σ121π-122π127σ128σ
16	39	126σ127σ128π-129π130σ132σ	126π127π128π-130π132σ134σ	126π127π128π-129π132σ133σ
17	**45**	132π138π143π-144π145π147π	140π141π143π-145π147π150σ	138π141π143π-144π147σ148π
18	46	123σ127π129π-130π134π135π	123σ127π129π-130π131π132π	122σ125σ129π-130π131π135σ
19	47	125π132π133π-134π135π137π	125π132π133π-134π135π138π	127σ130σ133π-134π135π137σ
20	48	126σ128π129π-130π133π134π	125σ126σ129π-130π131π134π	121σ122σ128π-130π131π133σ
21	49	122σ125π129π-130π131π132π	125π126π129π-130π131π134π	122σ126π129π-130π131π133π
22	50	131π132π133π-134π137π138π	129π131π133π-134π135π139π	127σ128σ132π-134π135π137π

$(HOMO-1)_1^*$ is a MO having a π nature in some molecules and σ nature in others. Figure 6 shows the $(HOMO-1)_1^*$ of molecules 19 and 37 [92].

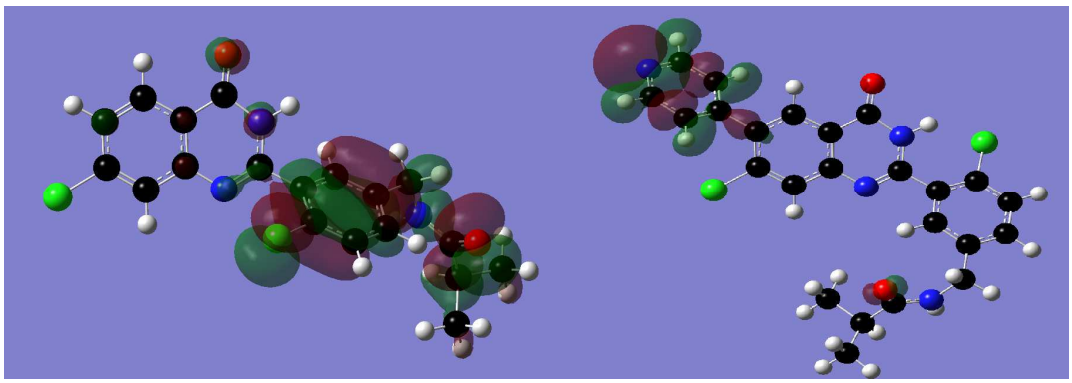

Figure 6. $(HOMO-1)_1^*$ of molecules 19 (left) and 37 (right). Isovalue of 0.02 e/au^3

$(HOMO)_1^*$ is of π nature in all the molecules. A high numerical value of $\left|S_1^E(HOMO-1)^*\right|$ strongly suggests that atom 1 can interact with an electron-deficient center. A corollary of this suggestion is that $(HOMO)_1^*$ should be of π nature for higher activity. A high value for $F_2(HOMO-1)^*$, a π MO in most molecules, indicates that atom 2 also interacts with an electron-deficient moiety. $(HOMO)_2^*$ is of π nature in all the molecules. Therefore, a $(HOMO-1)_2^*$ of π nature would be desirable. A high value for $\left|S_{13}^E\right|$ indicates that this atom interacts with an electron-deficient moiety. The vacant MO $(LUMO+1)_9^*$ has σ nature in almost all the molecules. A small value for $F_9(LUMO+1)^*$ is obtained only by diminishing the electron population of this MO. $(LUMO)_9^*$ is of π nature and has a high associated Fukui index. Therefore, there is the possibility that $(LUMO)_9^*$ might be interacting with an electron-rich center. $(HOMO-1)_9^*$ is a σ MO in almost all the molecules. A small value for $\left|S_9^E(HOMO-1)^*\right|$ is obtained by shifting the associated eigenvalue downwards in the energy axis. $(HOMO)_9^*$ is a π MO with a high associated Fukui index. To explain together these two simultaneous conditions for atom 9 we have two suggestions.

The first one involves the interaction of atom 9 with an electron-rich center through its first vacant MO and with an electron-deficient center through its first occupied MO. The other possibility is that, when the energy of $(HOMO-1)_9^*$ decreases, $(HOMO)_9^*$ will also lower its energy, making atom 9 a bad electron donor. In this case, atom 9 should interact with an electron-rich center through its $(LUMO)_9^*$. This last suggestion seems more likely. These suggestions are included in the partial two-dimensional (2D) inhibition pharmacophore shown in Fig. 7.

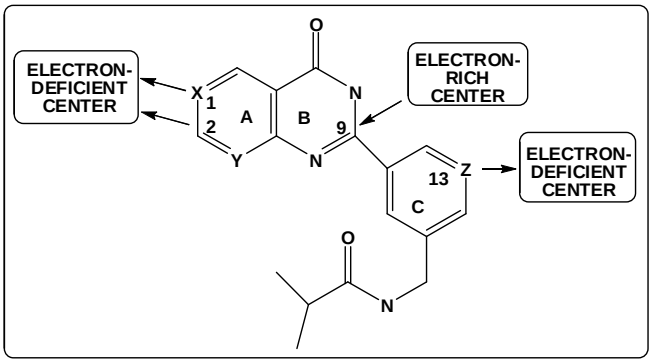

Figure 7. Partial 2D inhibition pharmacophore

This pharmacophore contains the conditions that are applicable to the whole set of molecules. The normal way to detect more variables is to employ a larger set in such a way as to be able to separate it into two or more subsets. Due to the small number of molecules studied here this is not possible.

To have a qualitative idea of the conformational flexibility of the side chain bonded to atom C15 (see Fig. 2), we show in Fig. 8 the superimposition of the ten lowest energy conformers of molecule 50. They were calculated with MarvinView (Dreiding force field) and superimposed with Hyperchem [93, 94].

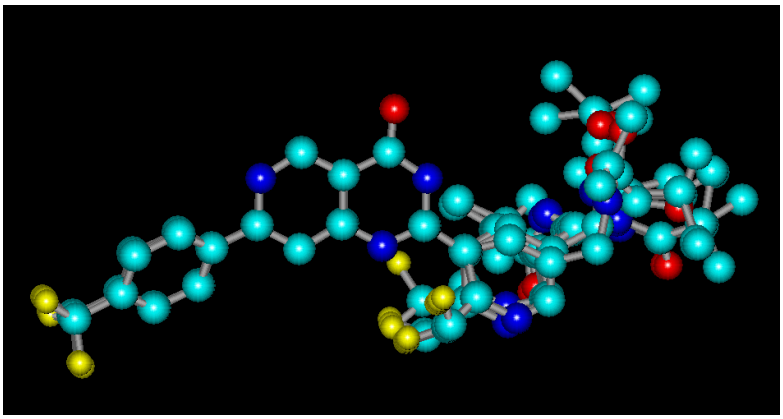

Figure 8. Superimposition of the ten lowest energy conformers of molecule 50

We can see that the side chain has rather high conformational flexibility. Aromatic ring C has a small degree of rotational freedom (see Fig. 2). Regarding the molecular electrostatic potential (MEP), Fig. 9 shows, respectively, the MEP maps of molecules 34 and 48 [92].

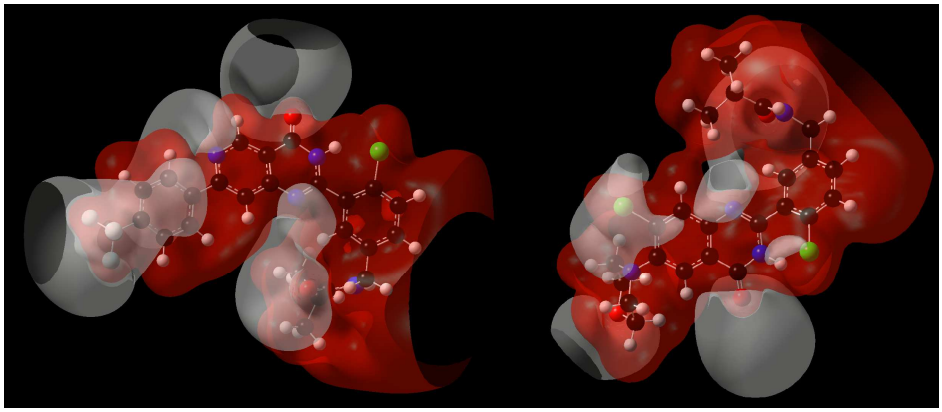

Figure 9. MEP maps of molecules 48 (left) and 34 (right). The white isovalue surface corresponds to negative MEP values (-0.01) and the red isovalue surface to positive MEP values (0.01)

We can see that the side chain is determinant in establishing the form of the MEP map at the right side of the molecule. We do not know what the exact conformation of each molecule is at moment of the *in vitro* measurements but we may speculate that the side chain could serve as an anchoring point for the ligand-site interaction.

It is our opinion that docking results, when not accompanied with other theoretical and/or experimental information, can provide little information *per se*. To build a docking model that is closer to physical reality we need to know the exact conditions inside the site and in the path leading to it (i.e., if there are water molecules, ions, etc. present, or not). Our results were obtained within the rigid ligand approximation and we expect that they, to be useful, should be compatible with the results of Eq. 2. If they are, they should provide qualitative information that cannot be obtained with our model-based method. Using the suggested interactions derived from the LMRA and docking results summarized in Table 4, we carried out a qualitative comparison of both shown in Table 5.

Table 5. Equivalence between LMRA and docking results

Atom	LMRA	Docking
Atom 1	Interaction with an electron-deficient center	39: C1-C from Arg-126A (3.93Å) 50: N1-N from His-72B (3.78Å) N1-N from Arg-126A (2.7Å)
C2	Interaction with an electron-deficient center	39: C2-C from His-72B (3.23Å) 50: C2-C from Arg-126A (3.67Å)
C9	Interaction with an electron-rich center	39: C9-N from Arg-73A (3.56Å) 50: C9-N from Leu-69B (5.56Å) C9-N from Arg-70A (5.44Å)
Atom 13	Interaction with an electron-deficient center	39: C13-C from Arg-73A (3.47Å) 50: N13-C from Arg-73A (3.09Å)
σ-σ interactions	None	39: C24-C from Leu-69A (4.36Å) 50: C24-C from His-72A(3.33Å) C24-C from Arg-73A (3.27Å) C23-C from Arg-73A (3.89Å)
Halogen bonds	None	50: F (from CF_3)-O from Tyr-130A (2.68Å) (?)

We can see that the docking results coincide, in a qualitative way, with the suggested interactions provided by Eq. 2. For both molecules the docking results allow a qualitative relationship to be drawn between the terms of Eq. 2 and some specific points of the site. Moreover, docking suggests the existence of σ interactions that the model based method could not detect because it did not include these atoms in the common skeleton. In Fig. 10 we show the superimposition of molecules 39 and 50 with the conformation they have when docked (see Figs. 4 and 5) [93]. Rings A and B were chosen as the common element for superimposition.

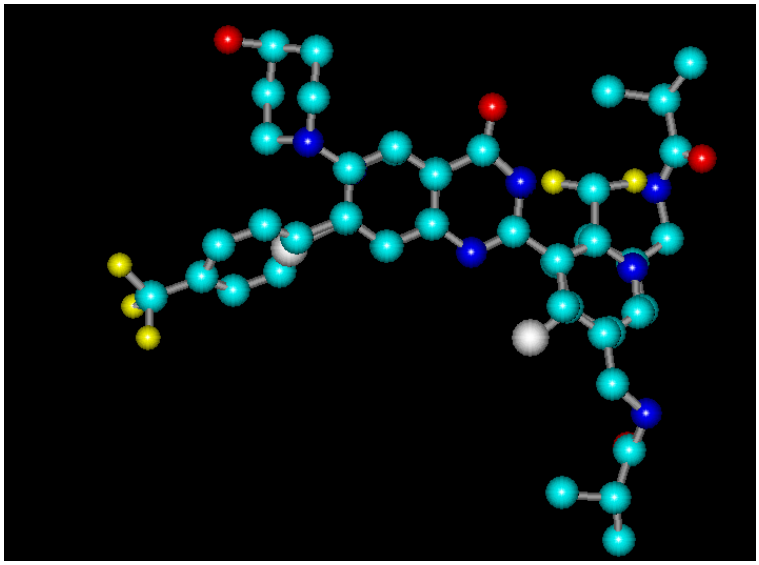

Figure 10. Superimposition of docked conformations of molecules 39 and 50

In molecule 50, the most active one, having an N1 atom instead of a C1, the side chain attached to C15 is pointing to the lower right hand side of the figure while in molecule 39 it is pointing to the upper side hand side. The experimental evidence strongly suggest that the replacement of C1 by N1 raises the inhibitory activity, a fact that nicely fits with the LMRA results indicating that this site interacts with an electron-deficient center. In turn this suggests that a substituent bonded to C1 should be an electron-rich one but separated from the ring by a CH_2 linker to avoid strong modifications of the electronic structure of the aromatic system (rings A and B). Perhaps a $–CH_2CN$ substituent should be useful for this goal. It is possible that docking studies might be ameliorated by working with flexible residues using exactly the same size and position of the 3D box and doing the docking for all the molecules analyzed.

In summary, we have found a good relationship between the electronic structures and inhibitory activities of a group of molecules against recombinant human mPGES-1. Our quantum-pharmacological results suggest specific interactions between some common skeleton atoms and unknown residues of the enzyme. Docking studies show what residues are available for these specific interactions and that these residues are not necessarily the same in all cases [82].

Acknowledgements
Prof. Dr. Bruce K. Cassels (Faculty of Sciences, University of Chile) is thanked for helpful comments.

REFERENCES

[1] D Ruan; S-P So, *Life Sci.*, **2014**, 116, 43-50.
[2] E Moilanen, *Basic Clin. Pharmacol. Toxicol.*, **2014**, 114, 2-6.
[3] F Millanta; P Asproni; A Canale; S Citi; A Poli, *Vet. Clin. Oncol.*, **2014**, DOI: 10.1111/vco.12096, n/a-n/a.
[4] S Zang; M Ni; Y Lian; Y Zhang; J Liu; A Huang, *Hum. Pathol.*, **2013**, 44, 1681-1687.
[5] H Idborg; P Olsson; P Leclerc; J Raouf; P-J Jakobsson; M Korotkova, *Prostagland. Other Lipid Mediat.*, **2013**, 107, 18-25.
[6] V Siljehav; A Olsson Hofstetter; P-J Jakobsson; E Herlenius, *Pediatr Res*, **2012**, 72, 460-467.
[7] C Hayashi; F Chisima; G Icikawa; M Suzuki; K Sugita; T Yamamoto, *J. Reprod. Immunol.*, **2012**, 94, 104.
[8] T Takemiya, *Neurochem. Int.*, **2011**, 59, 922-924.
[9] K Casós; L Siguero; M-T Fernández-Figueras; X León; M-P Sardá, et al., *Microvasc. Res.*, **2011**, 81, 261-268.
[10] H Kamata; K Hosono; T Suzuki; Y Ogawa; H Kubo, et al., *Biomed. Pharmacother.*, **2010**, 64, 409-416.
[11] Y Sasaki; D Kamei; Y Ishikawa; T Ishii; S Hara, *Chem. Phys. Lipds*, **2009**, 160, Supplement, S25.
[12] S Mattila; H Tuominen; J Koivukangas; F Stenbäck, *Neuropathol.*, **2009**, 29, 156-165.

[13] Y Kihara; T Matsushita; Y Kita; S Uematsu; S Akira, et al., *Proc. Natl. Acad. Sci. USA*, **2009**, 106, 21807-21812.
[14] S Hara; Y Kuroki, *Chem. Phys. Lipds*, **2009**, 160, Supplement, S9-S10.
[15] E Pecchi; M Dallaporta; A Jean; S Thirion; JD Troadec, *J. Neuroinmmunol.*, **2008**, 199, 104-114.
[16] N Elander; J Ungerbäck; H Olsson; S Uematsu; S Akira; P Söderkvist, *Biochem. Biophys. Res. Comm.*, **2008**, 372, 249-253.
[17] K Stark; H Törmä; EH Oliw, *Prostagland. Other Lipid Mediat.*, **2006**, 79, 114-125.
[18] Y Shi; L Cui; G Dai; J Chen; H Pan, et al., *Prostagland. Leukotr. Ess. Fatty Acids*, **2006**, 74, 309-315.
[19] M Nakanishi; V Gokhale; EJ Meuillet; DW Rosenberg, *Biochim.*, **2010**, 92, 660-664.
[20] RW Friesen; JA Mancini, *J. Med. Chem.*, **2008**, 51, 4059-4067.
[21] K Scholich; G Geisslinger, *Trends Pharmacol. Sci.*, **2006**, 27, 399-401.
[22] MG Chini; C Ferroni; V Cantone; P Dambruoso; G Varchi, et al., *MedChemComm*, **2015**, DOI: 10.1039/C4MD00319E
[23] M Verhoff; S Seitz; M Paul; SM Noha; J Jauch, et al., *J. Nat. Prod.*, **2014**, 77, 1445-1451.
[24] E Shang; Y Wu; P Liu; Y Liu; W Zhu, et al., *Bioorg. Med. Chem. Lett.*, **2014**, 24, 2764-2767.
[25] G Lauro; M Strocchia; S Terracciano; I Bruno; K Fischer, et al., *Eur. J. Med. Chem.*, **2014**, 80, 407-415.
[26] M Korotkova; P-J Jakobsson, *Basic Clin. Pharmacol. Toxicol.*, **2014**, 114, 64-69.
[27] A Banerjee; MY Pawar; S Patil; PS Yadav; PA Kadam, et al., *Bioorg. Med. Chem. Lett.*, **2014**, 24, 4838-4844.
[28] T Shiro; K Kakiguchi; H Takahashi; H Nagata; M Tobe, *Bioorg. Med. Chem.*, **2013**, 21, 2868-2878.
[29] T Shiro; K Kakiguchi; H Takahashi; H Nagata; M Tobe, *Bioorg. Med. Chem.*, **2013**, 21, 2068-2078.
[30] K Lee; VC Pham; MJ Choi; KJ Kim; K-T Lee, et al., *Bioorg. Med. Chem. Lett.*, **2013**, 23, 75-80.
[31] N Kablaoui; S Patel; J Shao; D Demian; K Hoffmaster, et al., *Bioorg. Med. Chem. Lett.*, **2013**, 23, 907-911.
[32] T Hanke; F Rörsch; TM Thieme; N Ferreiros; G Schneider, et al., *Bioorg. Med. Chem.*, **2013**, 21, 7874-7883.
[33] T Hanke; F Dehm; S Liening; S-D Popella; J Maczewsky, et al., *J. Med. Chem.*, **2013**, 56, 9031-9044.
[34] A Wiegard; W Hanekamp; K Griessbach; J Fabian; M Lehr, *Eur. J. Med. Chem.*, **2012**, 48, 153-163.
[35] T Shiro; H Takahashi; K Kakiguchi; Y Inoue; K Masuda, et al., *Bioorg. Med. Chem. Lett.*, **2012**, 22, 285-288.
[36] F Rörsch; El Buscató; K Deckmann; G Schneider; M Schubert-Zsilavecz, et al., *J. Med. Chem.*, **2012**, 55, 3792-3803.
[37] S-J Park; S-G Han; HM Ahsan; K Lee; JY Lee, et al., *Bioorg. Med. Chem. Lett.*, **2012**, 22, 7335-7339.
[38] R De Simone; I Bruno; R Riccio; K Stadler; J Bauer, et al., *Bioorg. Med. Chem.*, **2012**, 20, 5012-5016.
[39] MG Chini; R De Simone; I Bruno; R Riccio; F Dehm, et al., *Eur. J. Med. Chem.*, **2012**, 54, 311-323.
[40] J Bauer; B Waltenberger; SM Noha; D Schuster; JM Rollinger, et al., *ChemMedChem*, **2012**, 7, 2077-2081.
[41] B Waltenberger; K Wiechmann; J Bauer; P Markt; SM Noha, et al., *J. Med. Chem.*, **2011**, 54, 3163-3174.
[42] A Hamza; X Zhao; M Tong; H-H Tai; C-G Zhan, *Bioorg. Med. Chem.*, **2011**, 19, 6077-6086.
[43] C Greiner; H Zettl; A Koeberle; C Pergola; H Northoff, et al., *Bioorg. Med. Chem.*, **2011**, 19, 3394-3401.
[44] R De Simone; MG Chini; I Bruno; R Riccio; D Mueller, et al., *J. Med. Chem.*, **2011**, 54, 1565-1575.
[45] TYH Wu; H Juteau; Y Ducharme; RW Friesen; S Guiral, et al., *Bioorg. Med. Chem. Lett.*, **2010**, 20, 6978-6982.
[46] J Wang; D Limburg; J Carter; G Mbalaviele; J Gierse; M Vazquez, *Bioorg. Med. Chem. Lett.*, **2010**, 20, 1604-1609.
[47] AJ Liedtke; PRWEF Keck; F Lehmann; A Koeberle; O Werz; SA Laufer, *J. Med. Chem.*, **2009**, 52, 4968-4972.
[48] A Koeberle; E-M Haberl; A Rossi; C Pergola; F Dehm, et al., *Bioorg. Med. Chem.*, **2009**, 17, 7924-7932.
[49] CY-C Chen, *J. Taiwan Inst. Chem. Engin.*, **2009**, 40, 155-161.
[50] A Koeberle; H Zettl; C Greiner; M Wurglics; M Schubert-Zsilavecz; O Werz, *J. Med. Chem.*, **2008**, 51, 8068-8076.
[51] B Côté; L Boulet; C Brideau; D Claveau; D Ethier, et al., *Bioorg. Med. Chem. Lett.*, **2007**, 17, 6816-6820.
[52] MDM AbdulHameed; A Hamza; J Liu; X Huang; C-G Zhan, *J. Chem. Inf. Mod.*, **2007**, 48, 179-185.
[53] D Riendeau; R Aspiotis; D Ethier; Y Gareau; EL Grimm, et al., *Bioorg. Med. Chem. Lett.*, **2005**, 15, 3352-3355.
[54] YC Martin, *Quantitative drug design: a critical introduction*, M. Dekker, New York, 1978.
[55] JS Gómez Jeria, *Boll. Chim. Farmac.*, **1982**, 121, 619-625.
[56] JS Gómez-Jeria, *Int. J. Quant. Chem.*, **1983**, 23, 1969-1972.
[57] JS Gómez-Jeria, "Modeling the Drug-Receptor Interaction in Quantum Pharmacology," in *Molecules in Physics, Chemistry, and Biology*, J. Maruani Ed., vol. 4, pp. 215-231, Springer Netherlands, **1989**.
[58] JS Gómez-Jeria; M Ojeda-Vergara; C Donoso-Espinoza, *Mol. Engn.*, **1995**, 5, 391-401.

[59] JS Gómez-Jeria; M Ojeda-Vergara, *J. Chil. Chem. Soc.*, **2003**, 48, 119-124.
[60] JS Gómez-Jeria, *Elements of Molecular Electronic Pharmacology (in Spanish)*, Ediciones Sokar, Santiago de Chile, **2013**.
[61] JS Gómez-Jeria, *Canad. Chem. Trans.*, **2013**, 1, 25-55.
[62] JS Gómez-Jeria; M Flores-Catalán, *Canad. Chem. Trans.*, **2013**, 1, 215-237.
[63] A Paz de la Vega; DA Alarcón; JS Gómez-Jeria, *J. Chil. Chem. Soc.*, **2013**, 58, 1842-1851.
[64] I Reyes-Díaz; JS Gómez-Jeria, *J. Comput. Methods Drug Des.*, **2013**, 3, 11-21.
[65] JS Gómez-Jeria, *Int. Res. J. Pure App. Chem.*, **2014**, 4, 270-291.
[66] JS Gómez-Jeria, *Der Pharm. Lett.*, **2014**, 6., 95-104.
[67] JS Gómez-Jeria, *Brit. Microbiol. Res. J.*, **2014**, 4, 968-987.
[68] JS Gómez-Jeria, *SOP Trans. Phys. Chem.*, **2014**, 1, 10-28.
[69] JS Gómez-Jeria, *Der Pharma Chem.*, **2014**, 6, 64-77.
[70] JS Gómez-Jeria, *Res. J. Pharmac. Biol. Chem. Sci.*, **2014**, 5, 2124-2142.
[71] JS Gómez-Jeria, *J. Comput. Methods Drug Des.*, **2014**, 4, 32-44.
[72] JS Gómez-Jeria, *Res. J. Pharmac. Biol. Chem. Sci.*, **2014**, 5, 424-436.
[73] JS Gómez-Jeria, *J. Comput. Methods Drug Des.*, **2014**, 4, 38-47.
[74] JS Gómez-Jeria, *Res. J. Pharmac. Biol. Chem. Sci.*, **2014**, 5, 780-792.
[75] JS Gómez-Jeria; J Molina-Hidalgo, *J. Comput. Methods Drug Des.*, **2014**, 4, 1-9.
[76] JS Gómez-Jeria; J Valdebenito-Gamboa, *Der Pharma Chem.*, **2014**, 6, 383-406.
[77] D Muñoz-Gacitúa; JS Gómez-Jeria, *J. Comput. Methods Drug Des.*, **2014**, 4, 33-47.
[78] D Muñoz-Gacitúa; JS Gómez-Jeria, *J. Comput. Methods Drug Des.*, **2014**, 4, 48-63.
[79] DI Pino-Ramírez; JS Gómez-Jeria, *Amer. Chem. Sci. J.*, **2014**, 4, 554-575.
[80] F Salgado-Valdés; JS Gómez-Jeria, *J. Quant. Chem.*, **2014**, 2014 Article ID 431432, 1-15.
[81] R Solís-Gutiérrez; JS Gómez-Jeria, *Res. J. Pharmac. Biol. Chem. Sci.*, **2014**, 5, 1401-1416.
[82] JS Gómez-Jeria; A Robles-Navarro, *Res. J. Pharmac. Biol. Chem. Sci.*, **2015**, 6, In press.
[83] MJ Frisch; GW Trucks; HB Schlegel; GE Scuseria; MA Robb, et al., Gaussian98 Rev. A.11.3, Gaussian, Pittsburgh, PA, USA, **2002**.
[84] JS Gómez-Jeria, D-Cent-QSAR: A program to generate Local Atomic Reactivity Indices from Gaussian log files. 1.0, Santiago, Chile, **2014**.
[85] JS Gómez-Jeria, *J. Chil. Chem. Soc.*, **2009**, 54, 482-485.
[86] T Bruna-Larenas; JS Gómez-Jeria, *Int. J. Med. Chem.*, **2012**, 2012 Article ID 682495, 1-16.
[87] Statsoft, Statistica 8.0, 2300 East 14 th St. Tulsa, OK 74104, USA, **1984**-2007.
[88] U Varetto, Molekel 5.4.0.8, Swiss National Supercomputing Centre: Lugano, Switzerland, 2008.
[89] GM Morris; R Huey; AJ Olson, "Using AutoDock for Ligand-Receptor Docking," in *Current Protocols in Bioinformatics*, John Wiley & Sons, Inc., **2002**.
[90] GM Morris; R Huey; W Lindstrom; MF Sanner; RK Belew, et al., *J. Comput. Chem.*, **2009**, 30, 2785-2791.
[91] K Fukui; H Fujimoto, *Frontier orbitals and reaction paths: selected papers of Kenichi Fukui*, World Scientific, Singapore; River Edge, N.J., **1997**.
[92] RD Dennington; TA Keith; JM Millam, GaussView 5.0.8, GaussView 5.0.8, 340 Quinnipiac St., Bldg. 40, Wallingford, CT 06492, USA, **2000**-2008.
[93] Hypercube, Hyperchem 7.01, 419 Phillip St., Waterloo, Ontario, Canada, **2002**.
[94] Chemaxon, MarvinView, www.chemaxon.com, USA, **2014**.